



Electronic structure and photocatalytic properties of Ag–La codoped CaTiO_3

Hongjie Zhang^{a,*}, Gang Chen^{a,*}, Xiaodong He^b, Jing Xu^c

^a Department of Chemistry, Harbin Institute of Technology, Harbin 150001, China

^b School of Astronautics, Harbin Institute of Technology, Harbin 150001, China

^c Heilongjiang Institute of Technology, Department of Materials and Chemistry Engineering, Harbin 150001, China

ARTICLE INFO

Article history:

Received 6 September 2011

Received in revised form

28 November 2011

Accepted 28 November 2011

Available online 6 December 2011

Keywords:

Codoped

Photocatalytic activity

Hydrogen evolution

Visible light

ABSTRACT

Recently, ion-codoped semiconductor systems have been employed as photocatalysts with the objective of improving their photocatalytic activities under visible-light irradiation. In this paper, the effects of monovalence silver ion and trivalence lanthanum codoping into the photocatalytic activity of CaTiO_3 powder for overall water splitting were studied experimentally and theoretically. Pure and Ag–La codoped CaTiO_3 powder, prepared by sol–gel method which is assisted with ultrasonic technique for the first time, is further characterized by ultraviolet–visible (UV–vis) absorption spectroscopy. The UV–vis spectra indicate that the Ag^+ – La^{3+} ions doping not only enhanced the photocatalytic activity under ultraviolet–visible ($\lambda > 300 \text{ nm}$) light irradiation but also made the photocatalysts have visible light ($\lambda > 400 \text{ nm}$) response. Photocatalytic activity of codoped CaTiO_3 powder for hydrogen evolution under UV light is increased dramatically than that of pure CaTiO_3 powder when the doping amount is 3 mol%. The electronic structures of pure and codoped CaTiO_3 were investigated using density functional theory (DFT). The results of DFT calculation illuminate that the visible-light absorption bands in the Ag–La codoped CaTiO_3 catalyst are attributed to the band transition from the Ag 4d5s to the O 2p + Ti 3d hybrid orbital.

© 2011 Elsevier B.V. All rights reserved.

1. Introduction

The photocatalytic water splitting reaction driven by solar energy is one of the attractive targets due to the urgent demand of clean and renewable sources. Since TiO_2 electrode was first studied for water decomposition under UV-light in 1972 [1], several efforts have been made to improve the catalytic activity. Almost all of the photocatalysts developed in the past two decades have been composed of transition metal oxides involving octahedrally coordinated metal ions such as Ti^{4+} , Zr^{4+} , Nb^{5+} , and Ta^{5+} [2–4]. Among the vast majority of metal oxide photocatalysts, perovskite-type oxides are prominent for their broad diversity of properties. In an ABO_3 perovskite, varying the stoichiometry or doping with a cation of a different valence state can, in principle, change the electronic properties [5]. Therefore, one can control the composition of the constituent cations and can potentially alter the electronic structure originated from a donor or an acceptor level occurring in the forbidden band of a perovskite oxide by doping a foreign element. On the other hand, the doping of foreign elements into active photocatalysts with wide band gaps in order to make a donor or an acceptor level in the forbidden band is one of the effective ways in

the design of visible-light driven materials. There are many reports that the doped photocatalysts and semiconductor electrodes, such as TiO_2 [6–8] and SrTiO_3 [9–11] respond to visible light. CaTiO_3 (CTO), whose mineral name is perovskite, is one of the best-known wide gap oxides. The E_g of CTO is about 3.5 eV and the material is an insulator. However, careful donor-doping makes it conductive [12]. The low cost, the ease of synthesis of the material, and the extraordinarily high chemical stability against acids led us to consider its application as a photocatalyst in a wet environment [13].

The focus of this work was on the effects of silver and lanthanum codoped perovskite CaTiO_3 on photocatalytic properties. CaTiO_3 alone is active only under UV radiation, but the small amount doping of Ag and La ions can make CTO response to visible light. In the present study, the band structures and the photocatalytic properties of the perovskite-type materials CTO and Ag–La codoped CTO were investigated experimentally and theoretically, and the roles of Ag^+ and La^{3+} in the band structure were also discussed.

2. Experimental details

2.1. Preparation of materials

Ag–La codoped CaTiO_3 powder was prepared by a sol–gel method. In order to enhance the properties of the material, ultrasonic dispersing technique was used in this process. Tetrabutyl titanate was dissolved in 20 mL anhydrous ethanol under stirring, citric acid as chelating agent was added to tetrabutyl titanate solution under a constantly magnetic stirring or an ultrasonic dispersing. After stirring vigorously

* Corresponding authors. Fax: +86 451 86413753.

E-mail addresses: mis-hongjie@163.com (HJ. Zhang), gchen@hit.edu.cn (G. Chen).

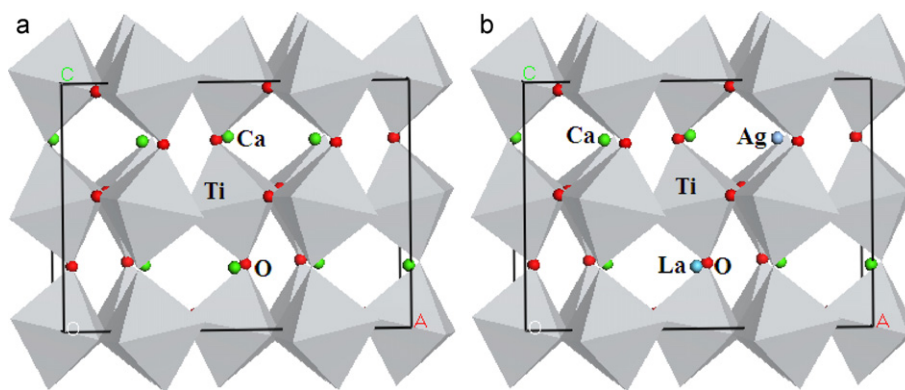


Fig. 1. The supercell crystal structure of CaTiO_3 : (a) pure CTO and (b) Ag–La codoped CTO.

or dispersing for about 30 min at room temperature, the mixed stoichiometrically solution of $\text{Ca}(\text{NO}_3)_2$, $\text{Ag}(\text{NO}_3)$ and $\text{La}(\text{NO}_3)_3$ was added drop-wise to the above titanium organic solution slowly to avoid tetrabutyl titanate hydrolyzing. The solution was kept under continuously stirring or dispersing at a temperature of 50°C until it became viscous, then the sol was transferred to an oven and dried at 120°C for 12 h to obtain the xerogel. When a dried gel was formed, it was burned by self-spread process in order to remove organic compounds and nitric acid. The burning remains were calcined at 850°C for 7–10 h for decarbonization and homogenization of the final samples.

2.2. Characterization of catalysts

The crystal structures of the sample powders were characterized by X-ray diffractometer (XRD) with $\text{CuK}\alpha$ radiation. The surface areas were determined by BET measurements (BF, ST2000). Diffuse reflection spectra were measured by UV–vis spectrometry (PG, TU-1900) to estimate band gaps of photocatalysts. The photocatalytic reactions proceed as follows: The photocatalyst powder (0.1 g) was dispersed in aqueous methanol solutions (volume ratio 1/20) (420 mL) by a magnetic stirrer in an outer irradiation quartz cell, which was connected to a closed gas-circulating system. The reactant solution was evacuated several times to ensure complete air removal, followed by irradiation under a 350 W high-pressure Hg lamp or 350 W high-pressure Xe lamp ($>400\text{ nm}$) via a Pyrex glass tube filled with NaNO_2 aqueous solution to block ultraviolet (UV) light [14]. Gas evolution was analyzed by gas chromatography (Agilent, GC-6820, TCD, Ar carrier).

The electronic band-structure calculation was based on the full-potential linear-muffin-tin-orbital (FP-LMTO) method [15], which uses the generalized gradient approximation (GGA) PW91 [16], an improvement of the local spin-density approximation (LSDA) within DFT [17] that is known to be an efficient and accurate scheme for solving the many-electron problem of a crystal. The density of the Monkhorst–Pack k -point mesh is $6 \times 6 \times 6$. The investigation is done using a supercell model based on the so-called large unit cell (LUC) approach [18], which has very high reliability for studies of doping in crystals. The two calcium atoms are replaced by impurity atoms of Ag and La, respectively, for CaTiO_3 crystals as shown in Fig. 1. A full geometry optimization is associated with the electronic structure calculation.

3. Results and discussion

3.1. Characterization of materials

XRD patterns of pure CaTiO_3 and Ag–La codoped calcium titanate are shown in Fig. 2. The pattern can be indexed to the CaTiO_3 orthorhombic host lattice phase only, and no impurities are detected. X-ray diffraction patterns of Ag–La codoped CTO powders are very similar to each other. A careful comparison of the (110) diffraction peaks in the range of 2θ 33.1° (Fig. 2b) showed that the peak positions are slightly shifted to higher angles with the increase in the amounts of doped Ag–La. The shift indicates that a part of Ag–La at least is homogeneously doped into the CaTiO_3 lattice. Ionic radii of La^{3+} (1.18 \AA) and Ag^+ (1.15 \AA) are closer to Ca^{2+} ion (1.00 \AA) than that of Ti^{4+} (0.68 \AA) which is at the position of B sites in perovskite structures. If Ti^{4+} is replaced by Ag^+ and La^{3+} , a large shift should be observed. Therefore, the

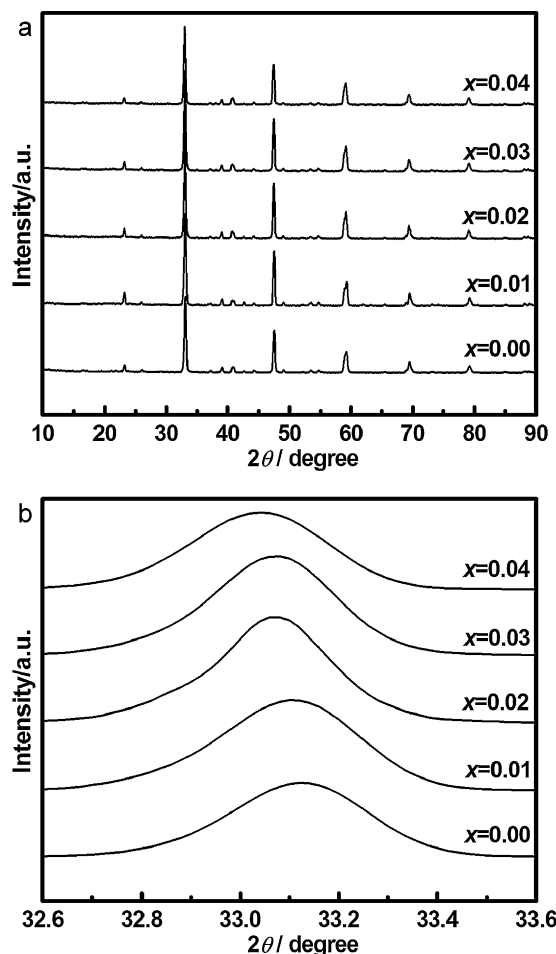


Fig. 2. X-ray diffraction patterns of (a) $\text{Ca}_{1-2x}\text{Ag}_x\text{La}_x\text{TiO}_3$ ($x=0.00-0.04$) and (b) X-ray diffraction peaks around 33.1° of $\text{Ca}_{1-2x}\text{Ag}_x\text{La}_x\text{TiO}_3$ ($x=0.00-0.04$).

small shifts to higher angles observed in the diffraction patterns of $\text{Ca}_{1-2x}\text{Ag}_x\text{La}_x\text{TiO}_3$ ($x=0.00-0.04$) suggest the substitution of Ag and La ions for Ca ions in the bulk which occupy A sites in perovskite structures.

3.2. UV–vis diffuse reflection spectra

Diffuse reflection spectra of the photocatalysts at room temperature are shown in Fig. 3. The reflectivity spectrum was transformed to absorbance intensity through Kubelka–Munk method. The onset of absorbance spectra of these photocatalysts show a shift to

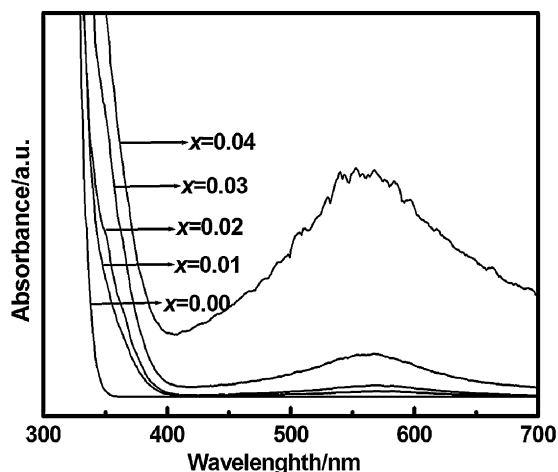


Fig. 3. UV-vis diffuse spectra of $\text{Ca}_{1-2x}\text{Ag}_x\text{La}_x\text{TiO}_3$ ($x = 0.00\text{--}0.04$).

longer wavelength with Ca^{2+} being substituted by Ag^+ and La^{3+} , the charge-transfer transition between Ag ion 4d5s electrons to the O 2p+Ti 3d hybrid orbital may explain the appearance of the red-shift. For the samples of Ag–La codoped CaTiO_3 , two types of absorption are generated in the visible light region, namely, a strong absorption in the UV region shorter than 360 nm, and a broad absorption extending into the visible region. Ag–La codoping in calcium titanate introduces a band in the visible region at <550 nm along with the main CTO peak at 360 nm. The absorption band at 550 nm is due to the transition of Ag 4d5s electrons to conduction band (CB).

3.3. Morphology

The typical SEM images of nondoped- CaTiO_3 and Ag–La codoped CaTiO_3 powders prepared by the same conditions are illustrated in Fig. 4. The images demonstrate that the material

shows irregular ball morphology. Compared with Fig. 4a–e, Ag–La codoped CaTiO_3 (see Fig. 4b–e) have significant influence on the morphologies of samples. The typical changes after Ag–La codoping are that the grain size becomes smaller. The small particle is advantageous for the photocatalytic activity. The decrease in the particle size probably cause a decrease in the migration distance of photogenerated electrons and holes to reach the reaction site on the surface, which probably contributes to the highly photocatalytic activities.

3.4. Band structure and photoabsorption properties

The band structure of Ag–La codoped CaTiO_3 with Ag and La at the Ca site (Fig. 1), which is the energetically preferable configuration, is displayed in Fig. 5c. For a comparison, those of undoped and Ag-doped CaTiO_3 are also plotted (Fig. 5a and b, respectively). The band structure of undoped CaTiO_3 displays a direct band gap about 2.45 eV at G (γ point). Although the calculated band gap of the undoped CaTiO_3 is underestimated compared with the experimental value (about 3.5 eV) due to the well-known limitation of GGA, the characteristics of the band structure as well as the relative variations of the band gap are expected to be qualitatively reasonable and reliable. A comparison of panels a and b in Fig. 5 shows that some unoccupied acceptor states are introduced above the valence band resulting in a band gap narrowing of about 0.23 eV, while the conduction band shows no significant change. The narrowed band gap may lead to the reduction of photon transition energy and thus redshifts of the optical absorption edge into the visible light region in Ag-doped CaTiO_3 . Furthermore, we must acknowledge that merely inducing visible light absorption does not guarantee satisfactory photocatalytic activity. It is pointed out that the Ag-doped CaTiO_3 displays a p-type conductivity character to keep charge balance (shown in Fig. 2b), whereas p-type conductivity in the oxide semiconductor with wide band gap is difficult to obtain, and these acceptor states are thermodynamically unstable [10]. Consequently, sliver-doping inevitably

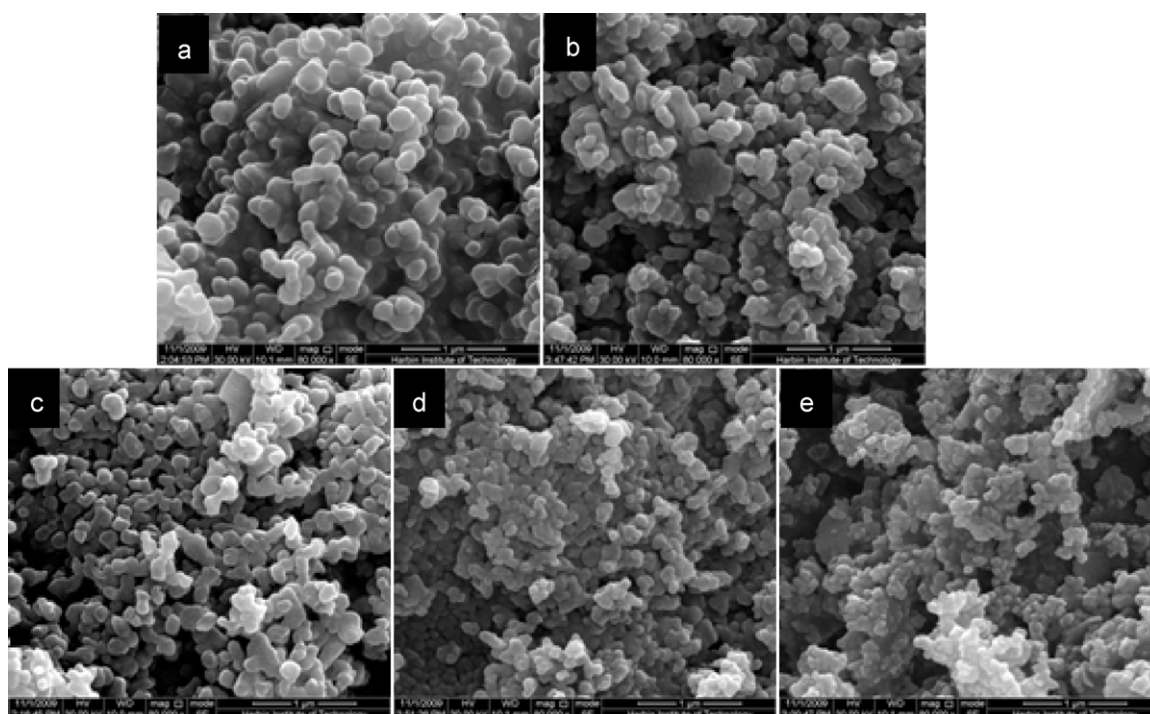


Fig. 4. SEM images of $\text{Ca}_{1-2x}\text{Ag}_x\text{La}_x\text{TiO}_3$: (a) $x = 0.00$, (b) $x = 0.01$, (c) $x = 0.02$, (d) $x = 0.03$, and (e) $x = 0.04$.

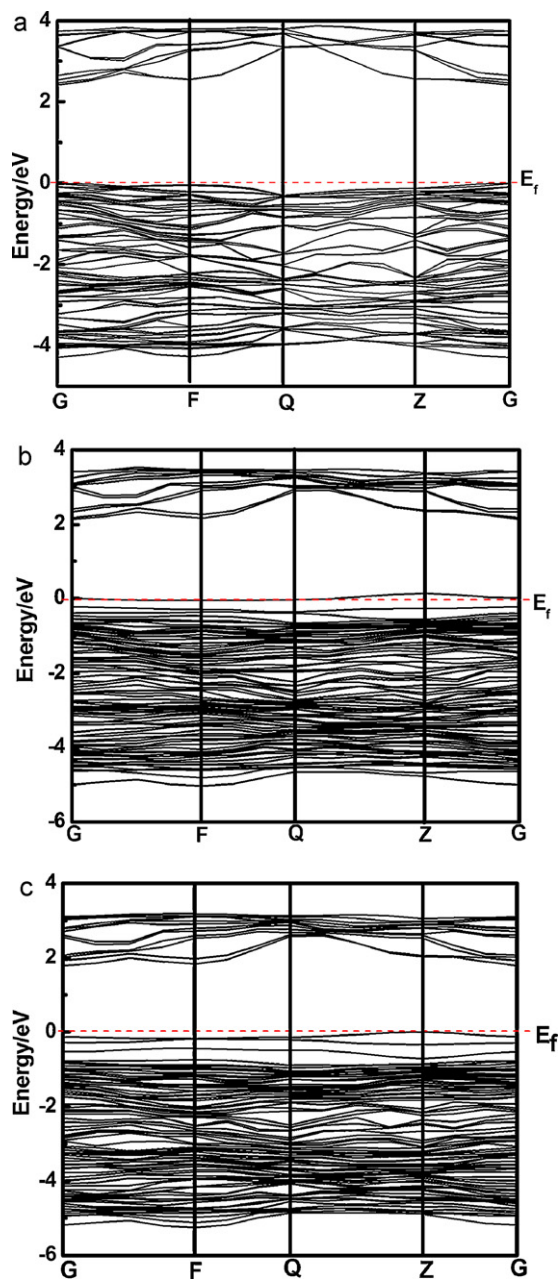


Fig. 5. Band structures of (a) CaTiO_3 , (b) CaTiO_3 doped with Ag, and (c) CaTiO_3 codoped with Ag-La.

introduces oxygen vacancies in the CaTiO_3 structure as a consequence of electron transfer from the Ti^{3+} states derived from oxygen vacancies to the partially occupied Ag 5s states during the sample preparation process. Nevertheless, oxygen vacancies always play an undesirable role as the recombination center of photogenerated electron-hole pairs during the photocatalytic reaction, which badly decreases the photocatalytic activity. Therefore, the sliver (p-type dopant) related defect bands must be passivated by another n-type dopant for the intent of effective photocatalytic activity. La is one of the promising candidates chosen for codoping with Ag. The band structure character of Ag-La codoped CaTiO_3 shown in Fig. 5c indicates that the bandwidth of the valence band is further expanded. The band gap narrows by about 0.55 eV compared with that of the undoped CaTiO_3 , which thus may lead to visible light responding. In this case, we can see that the valence band

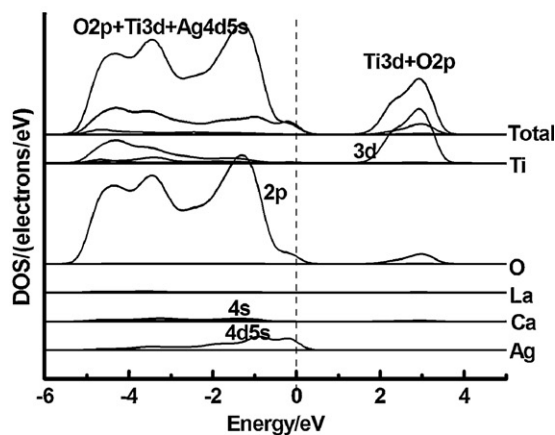
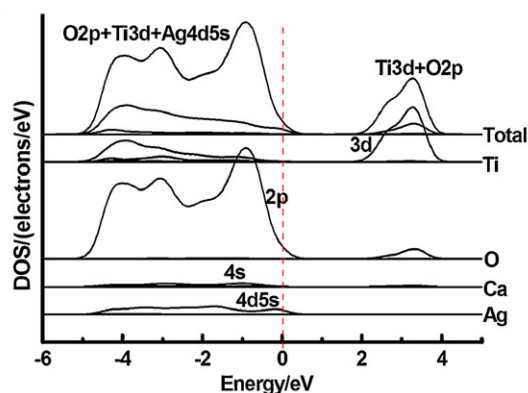
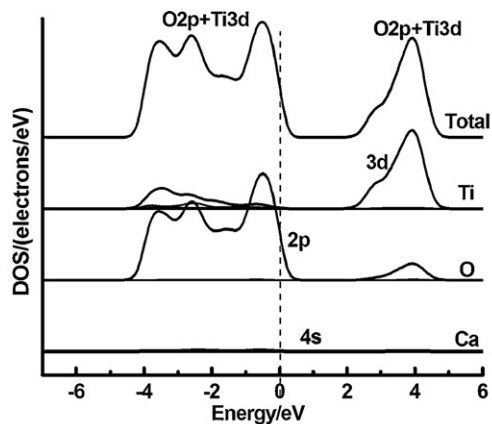


Fig. 6. DOS of (a) CaTiO_3 , (b) CaTiO_3 doped with Ag, and (c) CaTiO_3 codoped with Ag-La.

maximum increases greatly compared to the pure CaTiO_3 , whereas the change of conduction band is small indicating that the reducing ability is not reduced significantly. Furthermore, Fig. 5c also shows that the highest occupied level is pinned at the top of the valence band, which means that Ag-La codoping can keep the charge balance without the formation of undesired oxygen vacancies and eliminate the disadvantages aforementioned in the Ag-doped CaTiO_3 .

To examine the origin of the electronic structure modification, the projected DOS (density of states) plots of the Ag-La codoped CaTiO_3 are presented in Fig. 6c. The projected DOS plots of undoped CaTiO_3 and Ag-doped CaTiO_3 are also plotted in Fig. 5, panels a and b, respectively, as reference. For undoped CaTiO_3 , the upper valence band is dominantly composed of O 2p states and the conduction band Ti 3d states. Some Ti 3d states sufficiently disperse within

Table 1
BET surface area and H₂ evolution of Ca_{1–2x}Ag_xLa_xTiO₃.

Type of catalyst	Surface area (m ² g ⁻¹)	Activity (μmol h ⁻¹ gcat ⁻¹)	
		H ₂ /UV	H ₂ /vis
CaTiO ₃	9.64	325.4	0.0
Ca _{0.98} Ag _{0.01} La _{0.01} TiO ₃	10.61	549.6	2.6
Ca _{0.96} Ag _{0.02} La _{0.02} TiO ₃	11.39	1053.8	2.9
Ca _{0.94} Ag _{0.03} La _{0.03} TiO ₃	12.17	1064.2	10.1
Ca _{0.92} Ag _{0.04} La _{0.04} TiO ₃	11.44	436.9	4.1

the O 2p states illuminating the covalent property of the Ti–O bond. In addition, only a few Ca related electronic states appear in the O 2p valence band, which demonstrates ionic interaction between Ca and TiO₆. It is noted that the bandwidth of O 2p states in the upper valence band is about 4.25 eV. After the introduction of substitutional Ag for Ca (Fig. 6b), some Ag 5s partially occupied states are introduced above the valence band and overlap with O 2p states with the O 2p valence band expanded to be about 4.85 eV, which results in the band gap narrowing. Fig. 6c shows that the introduction of a La atom results in the O 2p valence band suffering a further expansion to be about 5.12 eV, whereas La related states have few contributions neither to the valence band nor to the conduction band due to the ionic interaction between La and TiO₆. In this situation, partially occupied Ag 5s states are present as totally occupied. To keep charge balance, this Ag atom requires one more electron from the CaTiO₃ lattice than a Ca atom does, so the Ag may act as a single acceptor. Meanwhile, the La atom releases one more electron than a Ca atom to the CaTiO₃ lattice and may act as single donor. Spontaneously, the extra electron brought by La dopant pairs up with the unpaired Ag 5s electron in CaTiO₃ lattice, namely, the electron on the donor level passivates the same amount of hole on the acceptor level, so that, this codoped system can still be of semiconductor character. Neither acceptor levels nor donor levels appearing within the band gap also confirm that the charge balance is maintained owing to the codoping of Ag and La, and thus the photocatalytic activity under visible light can be improved to an extensive degree. The charge compensation process, Ti³⁺ (d1) change into Ti⁴⁺ (d0) and partially occupied Ag 5s states change into completely occupied, indicates a stabilizing effect. Subsequently, it can be deduced that there presents a donor-acceptor pair (DAP) recombination [19] in the Ag–La codoped CaTiO₃, in which both acceptor levels and donor levels do not appear within the band gap resulting in the codoped CaTiO₃ a tempting structure with a narrowed band gap and the recombination center of photogenerated carriers is suppressed. So the Ag–La codoped CaTiO₃ system possesses high photostability and high photocatalytic activity under visible light like reported in Refs. [9] and [10].

3.5. Photocatalytic activity for water splitting

The specific surface area (BET) and dependence of the photocatalytic activity of un-doped CaTiO₃ and Ag–La codoped CaTiO₃ under UV light and visible light on the doping amount are listed in Table 1. It can be seen from the table that the specific surface areas raise monotonously with the continuous increments of codoped Ag–La amounts, which agrees with the SEM results. The photocatalytic activity increased with increasing doping amount to a maximum at 3 mol%, above which the activity dropped gradually. It is well known that the concentration of the doped ions exists an optimal value. When the doped concentration is lower than optimal doped concentration, there are not enough capture traps of charge carriers in the semiconductor, so photocatalytic activity increased with increasing of doped concentration; When the doped concentration is higher than optimal doped concentration, recombination

rate will be increased with the average distance between capture traps is shorter, at the same time, because the solubility of doped ions in the CaTiO₃ is limited, the higher doped concentration can lead to enrichment of doped ions on the surface of catalyst, which makes the photocatalytic activity reduce. Photocatalytic activities of Ag–La codoped CaTiO₃ powder for hydrogen evolution under UV and visible light are increased dramatically than that of pure CaTiO₃ powder.

4. Conclusions

CaTiO₃ codoped with Ag–La, prepared by sol–gel method coupled with ultrasonic technique, was shown to be an effective photocatalyst for water splitting. Theoretical calculations and experimental studies have demonstrated that increase of photocatalytic activities both under UV and visible light are caused by the Ag–La codoping. Neither acceptor levels nor donor levels appearing within the band gap also confirm that the charge balance is maintained owing to the codoping of Ag and La, and thus the photocatalytic activity under visible light can be improved to an extensive degree.

Acknowledgements

This work was supported by the National Nature Science Foundation of China (20871036, 21071036), Natural Science Foundation of Heilongjiang Province (ZD201011), and China Postdoctoral Science Foundation (20100480982).

References

- [1] A. Fujishima, K. Honda, *Nature* 238 (1972) 37–38.
- [2] M.Y. Guo, M.K. Fung, F. Fang, X.Y. Chen, A.M.C. Ng, A.B. Djurišić, W.K. Chan, *J. Alloys Compd.* 509 (2011) 1328–1332.
- [3] J.X. Sun, G. Chen, Y.X. Li, C. Zhou, H.J. Zhang, *J. Alloys Compd.* 509 (2011) 1133–1137.
- [4] G.K. Zhang, J. Gong, H.H. Gan, F. Lü, *J. Alloys Compd.* 509 (2011) 9791–9797.
- [5] L.S. Ji, J.J. Li, W.P. Fang, *J. Alloys Compd.* 489 (2010) L13–L16.
- [6] G.Q. Wang, W. Lan, G.J. Han, Y. Wang, Q. Su, X.Q. Liu, *J. Alloys Compd.* 509 (2011) 4150–4153.
- [7] L.C. Ji, C.C. Wu, S. Han, N. Yao, Y.Y. Li, Z.B. Li, B. Chi, J. Pu, J. Li, *J. Alloys Compd.* 509 (2011) 6067–6071.
- [8] X. Liu, Z.Q. Liu, J. Zheng, X. Yan, D.D. Li, S. Chen, W. Chu, *J. Alloys Compd.* 509 (2011) 9970–9976.
- [9] T. Puangpetch, T. Sreethawong, S. Chavadej, *Int. J. Hydrogen Energy* 35 (2010) 6531–6540.
- [10] W.J. Dong, X.Y. Li, J. Yu, W.C. Guo, B.J. Li, L. Tan, C.R. Li, J.J. Shi, G. Wang, *Mater. Lett.* 67 (2012) 131–134.
- [11] T. Puangpetch, P. Sommakettarin, S. Chavadej, T. Sreethawong, *Int. J. Hydrogen Energy* 35 (2010) 12428–12442.
- [12] H.J. Zhang, G. Chen, Y.X. Li, Y.J. Teng, *Int. J. Hydrogen Energy* 35 (2010) 2713–2716.
- [13] K.A. Shimura, H. Miyayama, H. Yoshida, *Stud. Surf. Sci. Catal.* 175 (2010) 85–92.
- [14] Y.X. Li, G. Chen, Q. Wang, X. Wang, A.K. Zhou, Z.Y. Shen, *Adv. Funct. Mater.* 20 (2010) 3390–3398.
- [15] O. Jepsen, O.K. Andersen, A.R. Mackintosh, *Phys. Rev. B* 13 (1975) 3060–3083.
- [16] J.P. Perdew, K. Burke, M. Ernzerhof, *Phys. Rev. Lett.* 77 (1996) 3865–3868.
- [17] P. Hohenberg, W. Kohn, *Phys. Rev.* 136 (1964) B864–B871.
- [18] A. Shlgur, V. Stefanovich, *Phys. Rev. B* 42 (1990) 9664–9673.
- [19] W. Wei, Y. Dai, M. Guo, L. Yu, B.B. Huang, *J. Phys. Chem. C* 113 (2009) 15046–15050.